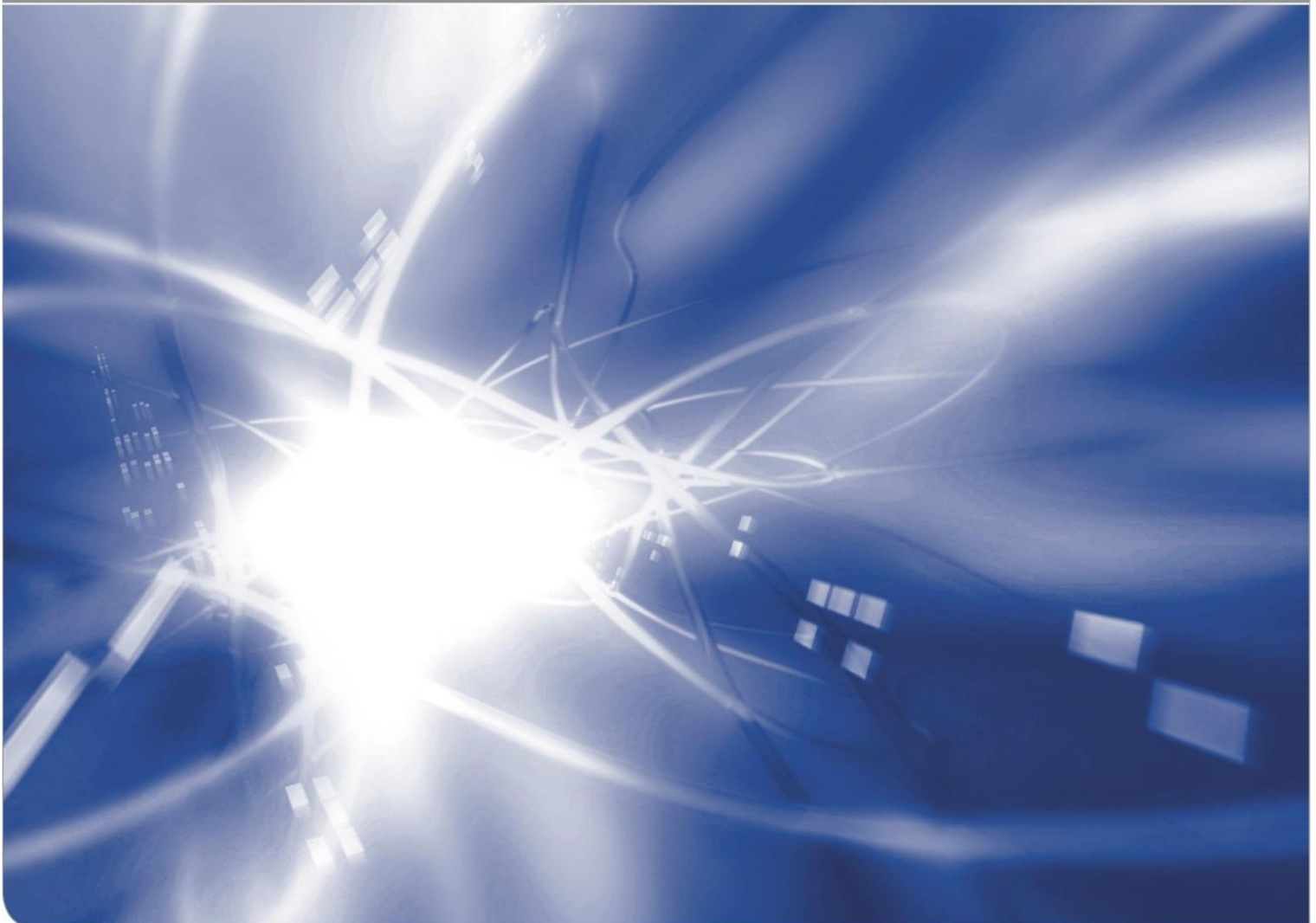


Tensile Stiffness of Laminated Segment Timber

by Lukas Windeck, Matthias Frese, Hans Joachim Blaß

KIT SCIENTIFIC WORKING PAPERS 167



**Research Centre for Steel, Timber and Masonry
Timber Structures and Building Construction**

R.-Baumeister-Platz 1
76131 Karlsruhe
Germany
<https://holz.vaka.kit.edu/>

Impressum

Karlsruher Institut für Technologie (KIT)
www.kit.edu



This document is licensed under the Creative Commons Attribution – Share Alike 4.0 International License (CC BY-SA 4.0): <https://creativecommons.org/licenses/by-sa/4.0/deed.en>

2021

ISSN: 2194-1629

Tensile Stiffness of Laminated Segment Timber

Lukas Windeck, Matthias Frese, Hans Joachim Blaß

Karlsruhe Institute of Technology – Timber Structures and Building Construction
windeck@kit.edu

Abstract. Laminated Segment Timber (LST) is an engineered wood product. It is panel-shaped and glued of trapezoidal spruce lamellas. As intermediate product, it is provided for the processing to layered LST, a glulam-like building material. The source material for LST are mechanically graded logs. This study aims at developing modelling and simulation techniques to assess the mechanical properties of LST. It is reported about 294 non-destructive tensile tests on specimens from LST and about the corresponding results. Digital image correlation was used to examine the tensile stiffness. Both global and local stiffness of the LST specimens were analysed in terms of tensile MOE. It was found that the local MOE of modelling units for LST can be predicted by the dynamic MOE of the source material and a newly developed knot ratio referring to the cross-section of LST specimens. Using this correlation, two stiffness models were derived for the local MOE. Their response shows good agreement with that of reference models from the literature. The models are, therefore, suitable for incorporation into a layered LST finite element model which is intended for predicting the mechanical properties.

1 Introduction

1.1 General and Objective

Laminated Segment Timber (LST) and layered LST are being technically developed by Stora Enso, Austria. Layered LST is a glulam-like secondary product composed of single LST layers. Both are engineered wood products made of spruce. Their structural application is being seen as an economic alternative to glulam. In contrast to boards for glulam, a segment cutting technique is used to produce trapezoidal cross-sections for LST.

At present, there are no strength and stiffness values available for LST. A comprehensive R&D project was therefore initiated. Its superior objective is to provide mechanical properties for the design of layered LST structures. The paper presents first results of experimental examinations on tensile properties. They are provided for the modelling of layered LST in order to obtain mechanical properties on the basis of finite element-based simulation techniques. Due to the affinity between layered LST and glulam, modelling approaches for glulam will be further developed and adapted to the new product.

1.2 LST Manufacture

Figure 1 illustrates the LST manufacture and that of secondary products like lengthwise finger jointed beams. After segment cutting and planing, a mutual gluing of the trapezoidal lamellas takes place resulting in panels. These LST panels are available in 90 to 160 mm depth in 10 mm increments. They can be cut in arbitrary width for further processing, e. g. to layered LST, see Figure 2, where single LST lamellas are glued on top of each other. Segment cutting increases the yield up to 85 % compared to traditional rectangular cutting with a yield of up to 65 % [1].

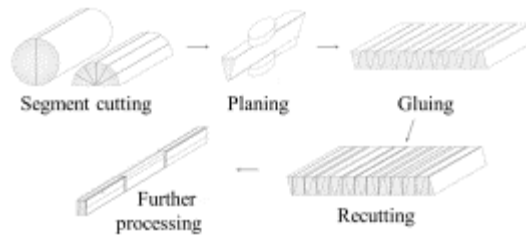


Figure 1 LST manufacture



Figure 2 Layered LST cross-section (120 x 270 mm, illustration turned by 90°) with 3 LST layers

2 Theoretical Fundamentals

2.1 Modelling and Simulation

Experimental tests in the necessary magnitude are too cost-intensive to determine stable statistical distributions of mechanical properties like the bending strength of glulam or of layered LST. Hence, a stochastic computational model is developed at Karlsruhe Institute of Technology (KIT) in order to simulate bending tests on layered LST beams. It is based on the fundamentals of the Karlsruhe Rechenmodell (KAREMO) [2–4]. KAREMO is a computational model which was developed in the 1980ies. It uses the finite element method to compute the local stresses in the modelled structure and finally returns load-carrying capacities. It is comprehensively validated and shows good agreement between computed bending strength values of large glulam members and experimental ones.

2.2 Tensile Stiffness for Glulam Modelling

Blass et al. [5] reflect the set of regression equations used for the empirical representation of material properties in the latest KAREMO version for glulam. The tensile MOE of board sections or board cells is calculated with eq. (1):

$$\ln(E_t) = 8.20 + 3.13 \cdot 10^{-3} \cdot \rho_0 - 1.17 \cdot \text{KAR} + \varepsilon \quad (1)$$

with $r = 0.77$ and $\varepsilon \in N(0, s_R)$ with $s_R = 0.180$

where s_R is the standard deviation of the error term ε . The model given by eq. (1) was derived by Glos, cf. [6]. It applies to cells containing clear wood as well as knots. Colling and Scherberger [7] found that the standard deviation s_R of the error term can be subdivided into two parts because the scattering of the MOE within a single board is lower than within the entire population or around the general regression line, see Figure 3. Hence, the part Δ_B of s_R describes the distance of the board to the general regression line. The scattering within a single board is described by $s_{R,B}$. For the given deviation of the error term $s_R = 0.180$ this allocation results in $\Delta_B = N(0;0.16)$ and $s_{R,B} = N(0.078;0.026)$ given by [8].

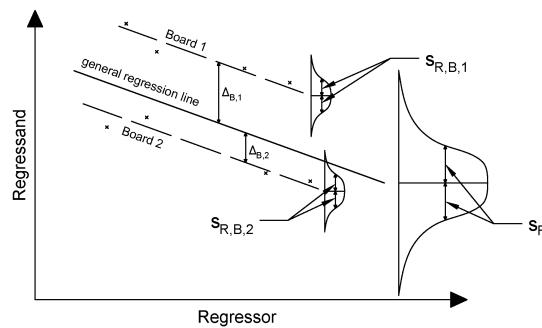


Figure 3 Allocation of the remaining total error [2]

2.3 Concept for layered LST

Like KAREMO, the computational model for layered LST uses a Monte-Carlo simulation for properties of single finite elements. That enables a probabilistic assessment of characteristic bending and tensile strength values by means of thousands of repeated computations. So far, KAREMO for glulam is a 2-D model because the influence of the width of the lamellas is considered implicitly by using the KAR value as predictor variable. However, since trapezoidal lamellas originating from different logs are systematically arranged in width direction of a LST panel, the computational model for layered LST was extended towards an advanced 3-D version. In order to determine the input data for the finite element simulation and to assess the influence of the different logs on the strength values, an easy-to-handle specimen with rectangular cross-section and an appropriate modelling unit were to be defined and examined. According to this idea, each LST beam was divided into three so called elementary lamellas (EL) as shown in Figure 4, left. Each of them consists of two half trapeziums where the originally adjacent half trapezium is part of the next elementary lamella.

2.4 Alternative Modelling

An analysis of the tensile stiffness on graded boards of Norway spruce from southern Germany was performed by Fink and Köhler, see [9]. The sample size was 200. 100 boards each were graded into the strength classes L25 and L40 according to

DIN EN 14081-4:2009 [10]. Two models to predict the tensile stiffness were developed: One describes the stiffness properties of clear wood sections (CWS); the other one can be used to calculate the MOE in sections with knots (KS), see eq. (2). Values for the model parameters are given in Table 1. In contrast to the study on LST, the CWS in their study had varying lengths. Both models are based on eigen frequency values of the boards. In case of KS, the tKAR value [9] is an additional predictor variable. Both models combined can be used to calculate a MOE that is constant for CWS over the entire board length. In areas where knots are present, the MOE is significantly reduced by the result of the second model.

$$\ln(E_{t,0,i}) = \beta_1 \cdot E_{\text{dyn},1} + \beta_2 \cdot \text{tKAR} + \beta_3 + \varepsilon \quad (2)$$

Table 1 Parameters for Fink's and Kohler's model/eq. (2)

Parameter	CWS	KS
β_1	$7.12 \cdot 10^{-5}$	$7.69 \cdot 10^{-5}$
β_2	0	-0.902
β_3	8.52	8.41
σ_ε	$5.47 \cdot 10^{-2}$	0.10

3 Materials and Methods

3.1 Raw Material and Elementary Lamellas

Prior to cutting the trapezoidal segments, the dynamic MOE of the spruce logs was determined by longitudinal vibrations through the manufacturer. Thereby, only logs with a dynamic MOE higher than 8500 N/mm² were processed to LST. Since merely 0.5 % of the logs had lower dynamic MOEs than this threshold, the resulting trapezoidal lamellas are essentially ungraded. The mean value of the dynamic log MOE amounted to 13280 N/mm² with a standard deviation of 1890 N/mm². According to the scheme in Figure 4, left, 300 ELs were cut off on a circular saw at KIT. The amount of ELs suitable for the further examinations was 294. 6 ELs were to be rejected due to cutting problems and deformations resulting from induced stresses during the manufacturing process. The final depth (d), and length (ℓ) of the examined elementary lamellas amounted to 90 mm and 2000 mm, respectively, whereas the width (b) had varying values in a range of 32 mm to 41 mm.

3.2 Preliminary Works and Definitions

The 294 elementary lamellas were to be tested in tension. It was intended to evaluate them systematically in terms of tensile stiffness and to find out any lengthwise distribution of structural properties and stiffness. The lamellas were, therefore, provided with a grid pattern in longitudinal sense with nine 150 mm long cells each, cf. Figure 5. That resulted in a total of 2646 cells. Based on this subdivision, the local MOE and global MOEs of cells and whole ELs, respectively, were determined.

The cell length corresponded to the gauge length of the cells. This gauge length differs from that in DIN EN 408:2012 [11], where five times the larger width is stipulated. In case of the elementary lamellas, this would result in 450 mm gauge length or rougher discretisation in terms of local MOE. However, for a finer discretisation as much as possible it was purposeful to reduce the gauge length to 150 mm and to match the grid pattern. Due to clamping at both ends, the total gauge length of an elementary lamella amounted to 1350 mm.

3.2.1 Knot measurement

The size of knots was determined. Due to the particular cross-sectional structure of elementary lamellas, no standard methods for knot size ratios, which capture the knottiness in squared timber, can be used. The criteria for a single knot of DIN 4074-1:2012 [12] were, therefore, adapted to the present case and the value EEL was established as knot size ratio for elementary lamellas. EEL is calculated with eq. (3) where the sum of $\max b_i$ is defined in Figure 4, right. $\max b_i$ is the respective maximum width of a knot appearing on the narrow side of the elementary lamella in each predefined cell. EEL was determined on all ELs. However, only knots with a diameter larger than 5 mm were considered.

$$EEL = \frac{\sum \max b_i}{2 \cdot b} \quad (3)$$

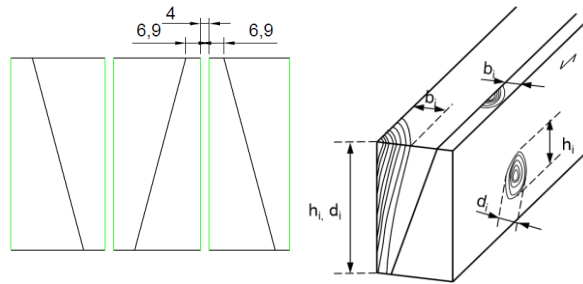


Figure 4 Left: Idealised division of an LST cross-section into three elementary lamellas. Right: Definitions for the knot size ratio EEL

3.2.2 Measurement of the eigen frequency and density

The eigen frequency f_0 of a longitudinal vibration of each EL was measured; the gross density ρ_{EL} of the whole EL was determined by its mass and dimensions. After testing, the density, the moisture content w , and the oven-dry density ρ_0 were measured. By means of the moisture content w the density ρ_{EL} was corrected to the oven-dry density $\rho_{EL,0}$. Based on the measurements, the corresponding dynamic MOE of each EL ($E_{dyn,EL}$) was calculated according to eq. (4), see [13] for a detailed description. The dynamic MOE represents an average value over the entire length of the lamella. It is comparable to a global MOE.

$$E_{dyn,EL} = (2 \cdot \ell \cdot f_0)^2 \cdot \rho \quad (4)$$

3.3 Test Procedure for the Tensile Stiffness

Digital image correlation (DIC) was used to track the relative movement during the tension tests and to measure the strain in each predefined cell of the elementary lamellas. Beforehand, a stochastic high contrast speckle pattern was applied by means of an airbrush system. Both narrow sides were tracked simultaneously, since the DIC system measures strains for the MOE only on the surface of the EL. That enabled the calculation of a mean value from the measurements of both opposite sides.

Additionally, data for the global MOE of the whole lamella was recorded. During testing, a maximum load of $F = 20$ kN was applied through clamping jaws with a speed of 5 kN/min. Figure 5 illustrates the principle of the test setup. It shows one pair of cameras in stereo setup provided for the one-sided measurement on the narrow side of nine cells. The other pair of cameras on the opposite side is not depicted.

The stereo setup enables the software to produce a 3D image of the measured surface. Hence, each point on the tracked surface can be viewed in a three dimensional space. For the evaluation of the MOE, only the strains in x-direction of the given coordinate system are used. Figure 6 shows an example of the strains in x-direction of one measured cell. This cell contains a knot with an EEL value of 0.44. It is visible that in the directly adjacent area around the knot the strains are considerably higher than in the surrounding clear wood, resulting in a reduced local MOE for this specific cell.

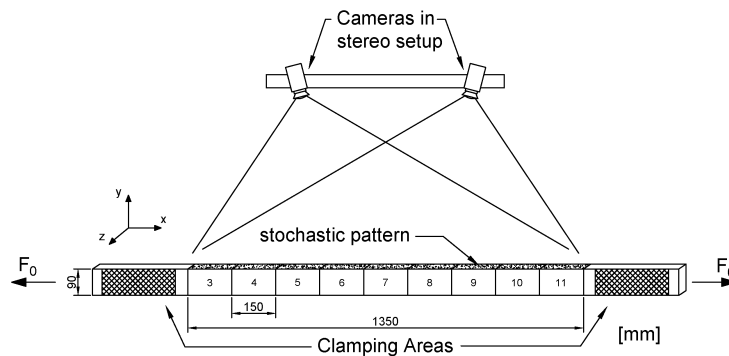


Figure 5 Schematic of the test setup for the determination of the tensile stiffness (only one side shown)

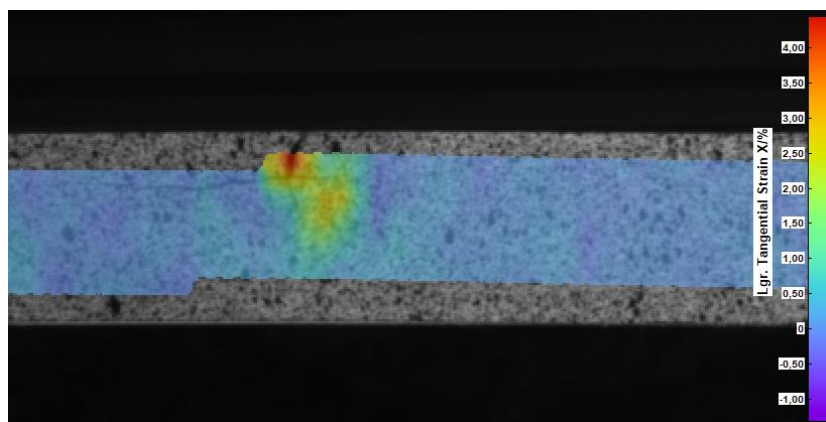


Figure 6 Local strains around a knot in an elementary lamella

Uniform stress distribution in a cross-section was assumed for the calculation of the local MOE in each cell. Figure 7 shows the stress-strain curves of one side of an EL. Due to knots in cell 4 and 11, the measured strains in these cells are significantly higher than the ones in the remaining 7 cells with clear wood. The evaluation of the MOE for each cell is based on the linear region of the determined stress-strain relationship. The same stress range was chosen for both sides of an EL. The global MOE was determined by means of a strain value measured over all 9 cells. For the calculation the same stress range as for the local MOE was used.

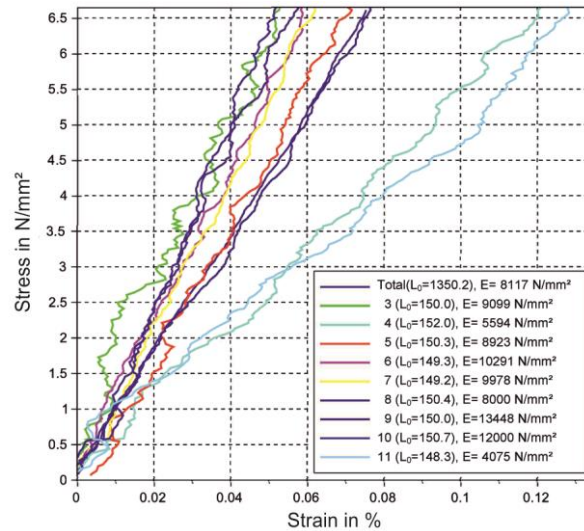


Figure 7 Stress-strain curves referring to the narrow side of an elementary lamella with a knot each in cell 4 and 11

4 Test Results

Taking the 2646 cells into account, the mean value and the standard deviation of the local MOE amounts to 12800 and 2836 N/mm², respectively. The minimum and maximum value is 2423 and 29040 N/mm², respectively. In contrast to the cells seen as a whole, the averaged standard deviation of the local MOE (calculated each with 9 cells of a single EL) amounts to 2310 which is lower than 2836 N/mm². Figure 8 shows the local MOE in dependence of the knot size ratio EEL. Histograms for both values are arranged beside the vertical and below the horizontal axis. The local MOE is approximately normally distributed and decreases with increasing knot size ratio EEL. The knot size ratio is right-skewed distributed. About 75 % of the cells have a knot size ratio of 0.0, and merely 1.5 % a ratio higher than 0.4. There is a gap between 0.0 and 0.05 without symbols, because only knots larger than 5 mm were recorded.

Figure 9 shows the correlation between local and global MOE as well as the frequency distribution of the global MOE which is approximately normally distributed. The mean value and the standard deviation amounts to 12348 and 1712 N/mm², respectively. The minimum and maximum value is 7629 and 16613 N/mm², respectively.

The mean oven-dry density ρ_0 was 411 kg/m³ with a standard deviation of 26.8 kg/m³. The mean moisture content was 10.8 % with a standard deviation of 0.6 %. All stated MOE values are corrected to the reference moisture content of 12 %.

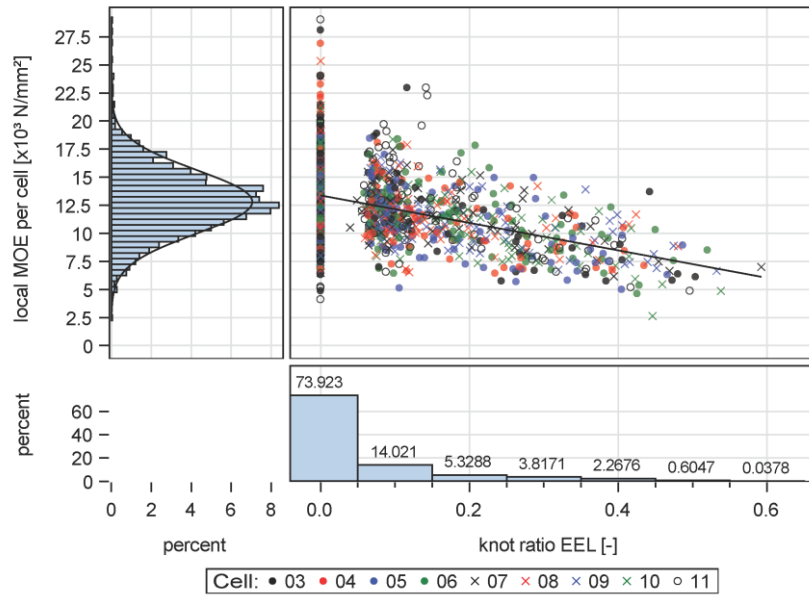


Figure 8 Local MOE in dependence of the knot size ratio EEL with corresponding distributions

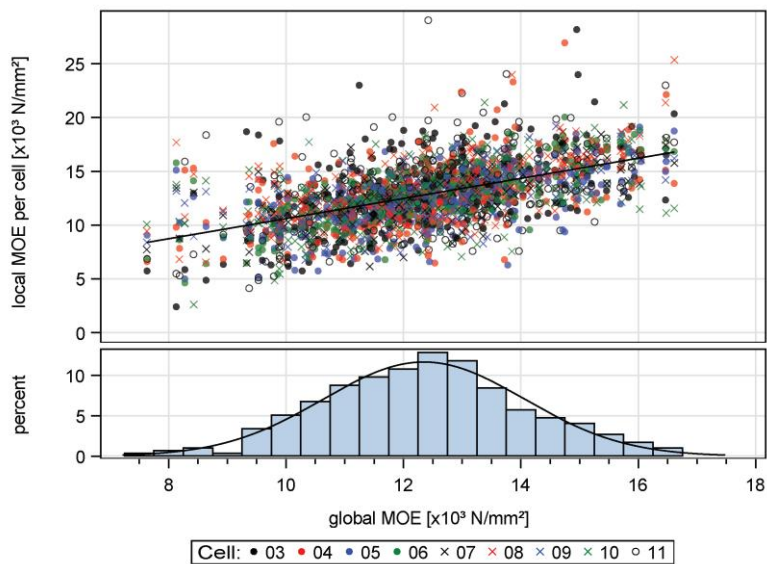


Figure 9 Correlation between local MOE and global MOE with density function of the measured global MOE

5 Models for the Tensile Stiffness

5.1 Global MOE

In order to improve the quality of the model for the global MOE, the sample size of 294 was extended with another 451 global MOE values originating from elementary lamellas provided for bending tests. However, the corresponding analysis will be the subject of a future publication. Due to the merged samples, in total 745 global MOE values are available. Hence, the statistics marginally changed: The mean global MOE and the standard deviation of the combined sample is 13442 and 2201 N/mm², respectively.

The dynamic MOE of the ELs ($E_{\text{dyn,EL}}$) is significantly correlated with the global static MOE ($E_{\text{t,0,glob}}$). The correlation coefficient amounts to $r = 0.87$. However, the dynamic MOE cannot be a suitable predictor variable for the global MOE. An elementary lamella was exclusively created for experimental examinations and considerations, and the structure of an EL does not exist as an independent object prior to any mechanical grading. Hence, it is impossible to grade them during manufacture. The following approach was therefore defined: As an elementary lamella consists of two half trapeziums, which have their origin in different logs, two dynamic log MOEs each effective in the EL can be used for the prediction of the stiffness. Since both trapeziums have the same share in the cross-section, the correlation with the mean dynamic MOE of both logs ($\bar{E}_{\text{dyn,log}}$) was tested on the global MOE of the ELs ($E_{\text{t,0,glob}}$). Figure 10 shows their mutual relationship. The correlation coefficient amounts to $r = 0.76$. Furthermore, the oven-dry density $\rho_{0,\text{EL}}$ is also a good predictor variable for the global MOE. The correlation coefficient amounts to $r = 0.573$. Though, a strong correlation between oven-dry density and dynamic MOE $\bar{E}_{\text{dyn,log}}$ also exists. Both predictor variables in the same regression model would result in multicollinearity, e.g [14]. In order to avoid that and to allow for the better correlation to the global MOE, merely the mean dynamic MOE is used in eq. (5) as predictor variable for the global MOE of ELs made of LST. The model is independent of the presence of knots within an elementary lamella.

$$E_{\text{t,0, glob}} = 1.256 \cdot \bar{E}_{\text{dyn, log}} - 2914 + \varepsilon \quad (5)$$

with $r = 0.76$ and $\varepsilon \in N(0,1413)$

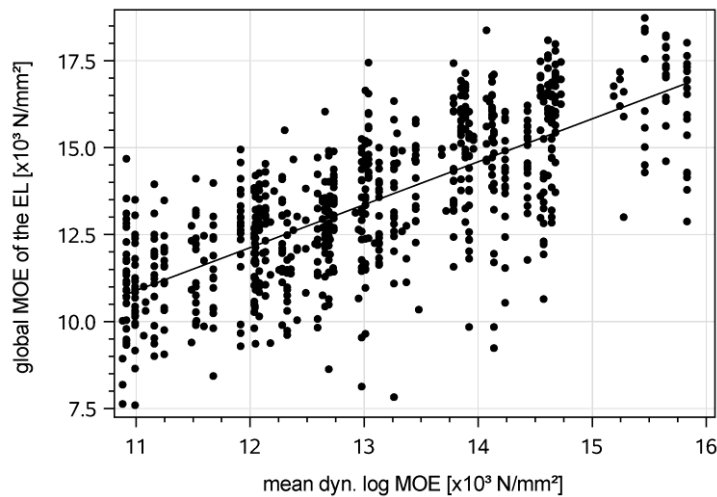


Figure 10 Global MOE of ELs and mean dynamic MOE of logs

5.2 Local MOE

5.2.1 Preliminary considerations

The global MOE and the knot size ratio EEL are suitable predictor variables for the local MOE which refers to individual cells 150 mm in length. Hence, they at least should be included in a regression model predicting the local MOE.

In order to find out whether further parameters like the oven-dry density ρ_0 have an influence on the local MOE, a correlation analysis was made. In contrast to Glos' model, however, no significant influence of the oven-dry density was found. It is noted that the oven-dry density of merely one cell was determined in this study and that examining the density of more than one cell can change that influence towards a stronger correlation. The two subsequent regression models for the local MOE, hereafter referred to as combined model, were derived on the basis of stiffness values obtained by the tensile tests. Local MOE values determined in the bending test were not used because they are effective in three consecutive cells and are, therefore, not local enough for the intended modelling. The two models follow Fink's and Kohler's principle [9]. Hence, it is differentiated between clear wood sections and those with knots. The total sample was subdivided into the sample A and B with 1954 and 692 cells, respectively, see Table 2 and Figure 11. The respective statistics obviously differ: Subsample A (1954 cells without knots) exhibits a lower standard deviation than that of the total sample and subsample B (692 cells with knots) a higher one than the total sample. For comparable purposes, a universal model based on data of the 2646 cells is also derived and proposed.

Table 2 Subsamples without and with knots

Sub-sample	Name	No. of cells	\bar{x} [N/mm ²]	s [N/mm ²]
CWS	A	1954	13344	2586
KS	B	692	11274	2912

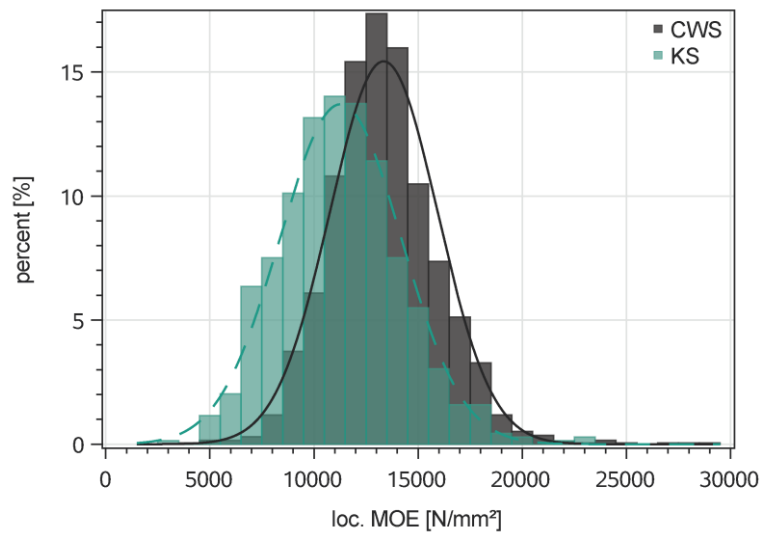


Figure 11 Frequency distributions of the local MOE of clear wood sections (CWS) and cells with knots (KS)

5.2.2 Combined model - CWS

The model for clear wood sections was derived without the knot size ratio EEL as predictor variable. In contrast to Fink's and Kohler's analysis, no mean stiffness of the CWS is calculated, but the individual local MOEs are predicted. A detailed analysis of

the stress-strain curves referring to the single cells of the tested ELs showed each an unstable strain line for the two outermost cells 03 and 11. This was due to the measurement configuration where the photographic lenses show decreasing focusing and precision in their periphery. Therefore, it was examined whether an exclusion of outermost cells would enhance the model but no significant change was found. Hence, the total number of 1954 cells in sample A were used in the regression analysis and eq. (6) was derived. It describes the individual local MOE of clear wood sections in elementary lamellas made of LST.

$$\ln(E_{t,0,loc,CWS}) = 6.56 \cdot 10^{-5} \cdot E_{t,0,glob} + 8.66 + \varepsilon$$

with $r = 0.60$ and $s_R = 0.143$ (6)

Due to the inhomogeneous structure of wood where two cells with the same global MOE have different local MOEs, an error term needs to be considered. The standard deviation of the error term ε in eq. (6) is $s_R = 0.143$. As stated in section 2.2, the standard deviation referring to cells within a board is lower than that of all tested cells. It was therefore checked whether this is also true for ungraded ELs. It was found that the distance of an EL Δ_{EL} to the general regression line can be described with $\Delta_{EL} = N(0;0.060)$. The remaining deviation within an EL can be described by $s_{R,EL} = N(0.137;0.052)$. Both values give evidence that the deviation within an EL is higher than the distance of an EL to the general regression line (0.137/0.060). The error term of each cell is calculated according to Colling's approach [2]:

- 1) For each EL a random distance Δ_{EL} from $N(0;0.060)$ is chosen.
- 2) For each EL a remaining deviation $s_{R,EL}$ from $N(0.137;0.052)$ is chosen.
- 3) For each CWS the predicted linear part of $E_{t,0,lok,CWS}$ is calculated according to eq. (6).
- 4) For each CWS of an EL a random value X_i from the remaining deviation $N(0; s_{R,EL})$ is chosen.
- 5) The final value of the local MOE is calculated according to eq. (7).

$$\ln(E_i) = E_{reg,i} + \Delta_{EL} + X_i \quad (7)$$

5.2.3 Combined model - cells with knots

A linear regression is based on the assumptions of normally distributed response variables and homoscedasticity meaning that the variance is constant throughout the range of the predictor variables, see e.g. [14]. However, Figure 8 shows a decreasing variance of local MOE with increasing values of EEL (heteroscedasticity). In order to stabilise the non-constant variance, the logarithm of the response variable is used. Since the local MOE of cells with knots highly depends on the knot size or rather the knot size ratio, the value EEL is included as second predictor variable. The regression analysis was performed with the 692 observations of sample B. Eq. (8) is the result. This model is provided for cells with knots.

$$\ln(E_{t,0,loc,KS}) = 7.30 \cdot 10^{-5} \cdot E_{t,0,glob} - 1.11 \cdot EEL + 8.60 + \varepsilon$$

with $r = 0.75$ and $s_R = 0.171$

(8)

The standard deviation of the error term ε is $s_R = 0.171$. It is also subdivided into two parts: $\Delta_{EL} = N(0;0.094)$ as distance of an EL to the general regression line and $s_{R,EL} = N(0.156;0.091)$ as remaining deviation within an EL. The same procedure described above applies to calculate local MOE values for KS of elementary lamellas.

5.2.4 Universal model

The universal model is derived to describe both clear wood sections and those with knots. The global MOE and the knot size ratio EEL are used as predictor variables. The result is eq. (9).

$$\ln(E_{t,0,loc}) = 6.80 \cdot 10^{-5} \cdot E_{t,0,glob} - 0.98 \cdot EEL + 8.63 + \varepsilon$$

with $r = 0.72$ and $s_R = 0.152$

(9)

The standard deviation of ε is $s_R = 0.152$. For the subdivision $\Delta_{EL} = N(0;0.043)$ and $s_{R,EL} = N(0.149;0.044)$ apply.

6 Discussion

It has been found out that the standard deviation of the local MOE (referring to a cell) within a single EL is lower than that of the whole sample of 2646 cells, see section 4. Hence, the subdivision of the error term into Δ_{EL} and $s_{R,EL}$ is in accordance with this finding. In terms of modelling, Δ_{EL} and $s_{R,EL}$ represent the distance to the general regression line and the remaining deviation within an EL, respectively. Although the variation of the local MOEs within an EL is comparably high, cf. Figure 9, its scattering is more or less independent of the level of the global MOE. The value range is nearly the same for the local and global MOE. Therefore, the averaged standard deviation of the local MOE within an EL needs to be lower than that of all the measured cells.

Figure 12, top shows an evaluation of the combined model based on the eqs. (6) and (8). The diagram exemplifies the predicted local MOE depending on the measured values. CWS are represented by black dots and knot sections by circles. In order to prove the quality of the model, error terms are not considered. In a range from 10E3 to 15E3 N/mm² the mean of the ratios is 1.008 with a standard deviation of 0.12. Hence, the MOE is predicted very well in this range. In case of lower MOEs the predicted values are (much) higher, and in case of higher MOEs the predicted ones are lower.

The green dots in Figure 12, top, represent a comparable evaluation of Glos' model. For the evaluation, the single value of the oven-dry density available per EL could be used for all cells of an EL because of the minor variance of the density in boards or ELs, see [8]. Since no KAR values could be determined for elementary lamellas, the knot size ratio EEL was inserted instead. The markers in green show a similar trend to the ones of the predicted values referring to the combined model. However, Glos' model deviates from measured values slightly more than the combined model does.

Figure 12, bottom, shows a comparison with Fink's and Kohler's model. Even here, EEL is used instead of KAR for the comparable evaluation. The MOEs of both cell types can be predicted very well, and only a minor difference between both models exists. Overall, for the here tested ELs, Fink's and Kohler's model shows a better fit than Glos' model. However, the combined model developed for the ELs provides the best agreement. All three examined models have in common that loc. MOE values higher than $18 \times 10^3 \text{ N/mm}^2$ cannot be calculated neglecting the error term.

Figure 13 compares the calculated linear parts of the universal model with the respective linear parts of the combined model. The values shown differ by cell type. For high MOEs and cells with knots, the universal model results in lower values than the combined model does, and for low MOEs, higher values are calculated. For clear wood sections, both models almost yield the same values. As the universal model underestimates high MOEs and overestimates low ones, it is not appropriate to represent the local MOE.

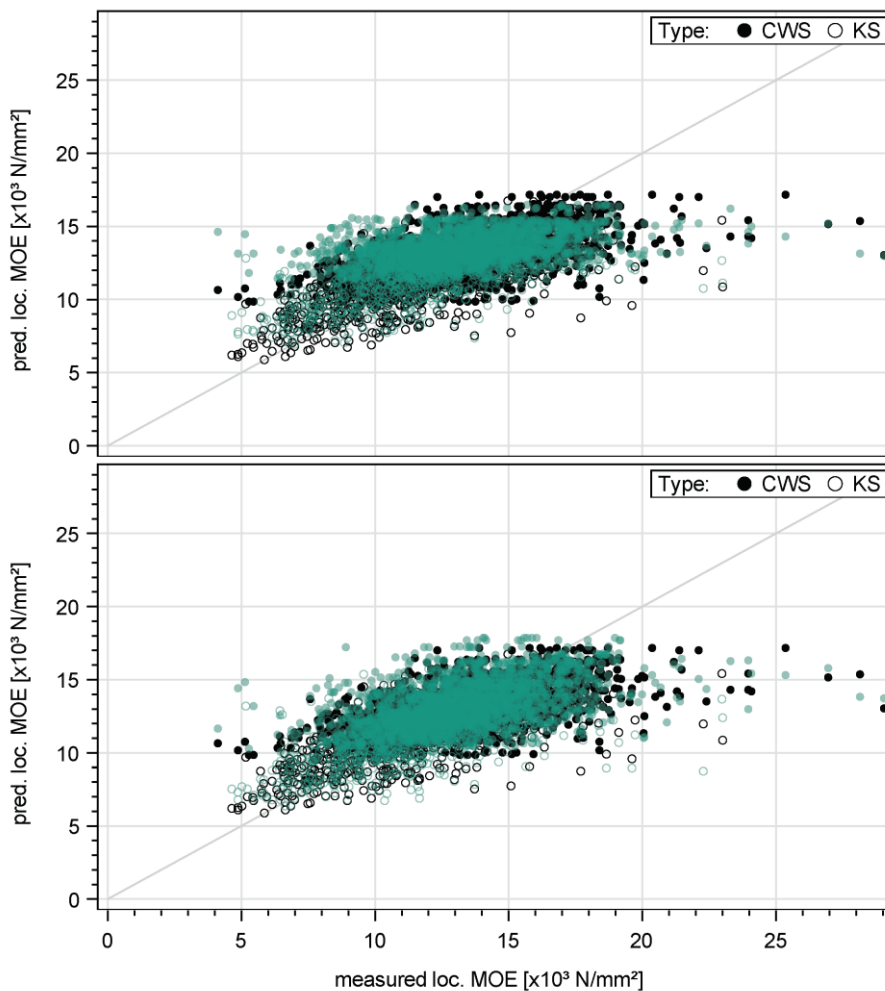


Figure 12 Comparison of predicted to measured MOEs. Top: combined model (black) and Glos' model (green). Bottom: Fink's and Kohler's model (green)

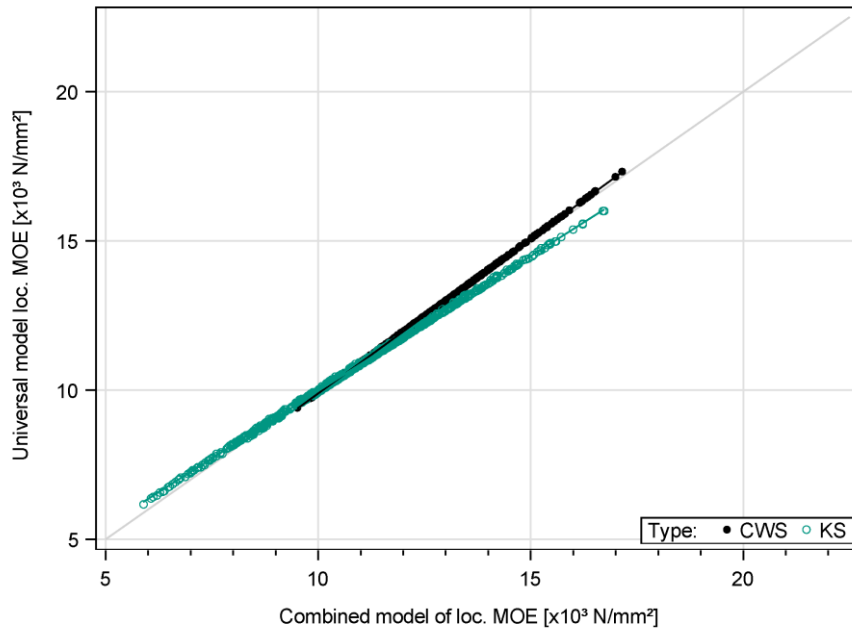


Figure 13 Comparison between universal and combined model

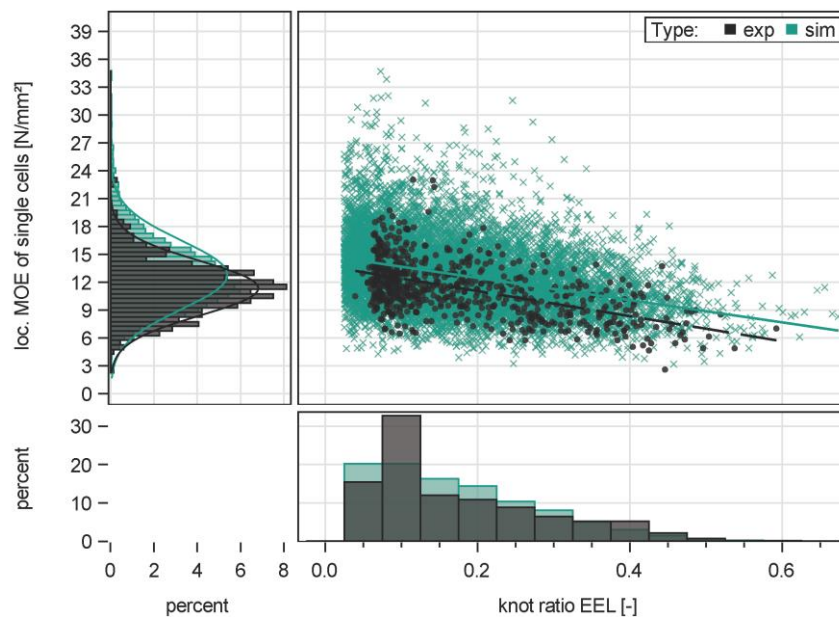


Figure 14 Comparison between simulated and experimental local MOEs

Taking into account the preceding model comparisons and discussions, the combined model is seen to be appropriate to represent the local MOE of cells in elementary lamellas. Figure 14 shows a comparison between almost 10000 simulated local MOEs (green) and the experimental ones (black). The modelled values originate from complete simulated elementary lamellas, but only cells with knots are pictured. Randomly distributed error terms were considered. The simulation shows that its general trend fits the experimental values quite well. However, the simulation overestimates the experimental mean value and the standard deviation. The histogram of the knot size ratio EEL shows deviations in the respective frequency distributions. It is, therefore, possible that the overestimation

results from the knot model used in the simulation. This issue will be the subject of future research.

7 Conclusions

The following conclusions can be drawn from this study:

- Experiences during the experimental examination of LST and glulam-like layered LST have proved that segment cutting is a promising new sawing technology to produce an economic engineering wood product.
- Modelling and simulation techniques developed for the prediction of mechanical properties of glulam can be basically adopted for layered LST. However, the three-dimensional structure of layered LST required a new approach.
- Essential differences between glulam and LST concern the basic modelling unit. In contrast to boards as modelling unit for glulam, so called elementary lamellas and an appropriate knot size ratio were to be defined. Elementary lamellas are composed of two glued trapezoidal battens to obtain an easy-to-handle rectangular cross-section.
- Digital image correlation and simultaneous tensile tests were successfully employed to examine the stiffness properties of elementary lamellas in terms of global and local stiffness.
- Based on the data obtained, models were developed to predict the tensile stiffness of sections in elementary lamellas. It was found that a combined model, where the stiffness of sections with and without knots is predicted independently of each other, is most suitable. Main drivers in the combined model are the dynamic log MOE available from strength grading and the newly defined knot size ratio for elementary lamellas.
- So far, the combined model will be used in a finite element model to analyse the bending strengths of large layered LST members.
- Future research will concern tensile and bending strength of finger joints and interaction between tensile and bending stress in cross-sections of elementary lamellas.

Annotation

This paper was accepted for publication on the occasion of the World Conference of Timber Engineering (WCTE) 2020 in Santiago, Chile. Due to the unforeseeable circumstances of the global pandemic, it was withdrawn as contribution to the WCTE and is published as KIT Working Paper instead. Further information on the manufacturing process and first results of simulated bending strengths are reported in [15].

8 Literaturverzeichnis

- [1] PINTO, I. ; KNAPIC, S. ; PEREIRA, H. ; USENIUS, A.: *Simulated and realised industrial yields in sawing of maritime pine (Pinus pinaster Ait.)*. In: *European Journal of Wood and Wood Products* 64 (2006), Nr. 1, S. 30–36

- [2] COLLING, F.: *Tragfähigkeit von Biegeträgern aus Brettschichtholz in Abhängigkeit von den festigkeitsrelevanten Einflußgrößen*. Universität Karlsruhe. Dissertation. 1990
- [3] FRESE, M. ; BLAß, H. J.: *Bending strength of spruce glulam*. In: *European Journal of Wood and Wood Products* 67 (2009), Nr. 3, S. 277–286
- [4] FRESE, M.: *Computergestützte Verfahren zur pragmatischen Beurteilung der Tragwiderstände von Brettschichtholz: Zusammenfassung exemplarischer Simulationsstudien*. Habilitation. Karlsruhe, 2016 (Karlsruher Berichte zum Ingenieurholzbau 31)
- [5] BLAß, H. J. ; FRESE, M. ; GLOS, P. ; DENZLER, J. ; LINSENMANN, P. ; RANTA-MAUNUS, A.: *Zuverlässigkeit von Fichten-Brettschichtholz mit modifiziertem Aufbau* : KIT Scientific Publishing, 2009
- [6] EHLBECK, J. ; COLLING, F. ; GÖRLACHER, R.: *Einfluß keilgezinkter Lamellen auf die Biegefestigkeit von Brettschichtholzträgern*. In: *Holz als Roh- und Werkstoff* 43 (1985), 333-337, 369-373, 439-442
- [7] COLLING, F. ; SCHERBERGER, M.: *Die Streuung des Elastizitätsmoduls in Brett-längsrichtung*. In: *Holz als Roh- und Werkstoff* 45 (1987), Nr. 3, S. 95–99
- [8] GÖRLACHER, R.: *Klassifizierung von Brettschichtholzlamellen durch Messung von Longitudinal-schwingungen*. Universität Karlsruhe. Dissertation. 1990
- [9] FINK, G. ; KÖHLER, J.: *Model for the prediction of the tensile strength and tensile stiffness of knot clusters within structural timber*. In: *European Journal of Wood and Wood Products* 72 (2014), Nr. 3, S. 331–341
- [10] DIN EN 14081-4. Oktober 2009. *Holzbauwerke – Nach Festigkeit sortiertes Bauholz für tragende Zwecke mit rechteckigem Querschnitt – Teil 4: Maschinelle Sortierung*
- [11] DIN EN 408. Oktober 2012. *Holzbauwerke - Bauholz für tragende Zwecke und Brettschichtholz - Bestimmung einiger physikalischer und mechanischer Eigenschaften*
- [12] DIN 4074-1. Juni 2012. *Sortierung von Holz nach der Tragfähigkeit - Teil 1: Nadelschnittholz*
- [13] GÖRLACHER, R.: *Ein neues Meßverfahren zur Bestimmung des Elastizitätsmoduls von Holz*. In: *Holz als Roh- und Werkstoff* 42 (1984), S. 219–222
- [14] CHATTERJEE, S. ; PRICE, B.: *Praxis der Regressionsanalyse*. 2. Aufl. München, Wien : Oldenbourg, 1995 (Lehr- und Handbücher der Statistik)
- [15] WINDECK, L. ; HIRMKE, M.: *Biegefestigkeit von Segmentlamellenholz*. In: *Bautechnik* 98 (2021), S1, S. 52–60

KIT Scientific Working Papers
ISSN 2194-1629

www.kit.edu